pH-Dependent Reduction Potentials and Proton-Coupled Electron Transfer Mechanisms in Hydrogen-Producing Nickel Molecular Electrocatalysts

ARTICLE *in* INORGANIC CHEMISTRY · MARCH 2013

Impact Factor: 4.76 · DOI: 10.1021/ic302056j · Source: PubMed

4 AUTHORS, INCLUDING:

Samantha Horvath
Illinois Rocstar LLC
20 PUBLICATIONS **249** CITATIONS

SEE PROFILE

Inorganic Chemistry

Article

pubs.acs.org/IC

pH-Dependent Reduction Potentials and Proton-Coupled Electron Transfer Mechanisms in Hydrogen-Producing Nickel Molecular Electrocatalysts

Samantha Horvath,[†] Laura E. Fernandez,[‡] Aaron M. Appel,[§] and Sharon Hammes-Schiffer*[,†]

[†]Department of Chemistry, 600 South Mathews Avenue, University of Illinois at Urbana−Champaign, Urbana, Illinois 61801, United States

[‡]Department of Chemistry, 104 Chemistry Building, Pennsylvania State University, University Park, Pennsylvania 16802, United States

[§]Center for Molecular Electrocatalysis, Pacific Northwest National Laboratory, P.O. Box 999, K2-57, Richland, Washington 99352, United States

Supporting Information

ABSTRACT: The nickel-based $P_2^{Ph}N_2^{Bn}$ electrocatalysts comprised of a nickel atom and two 1,5-dibenzyl-3,7-diphenyl-1,5-diaza-3,7-diphosphacyclooctane ligands catalyze H_2 production in acetonitrile. Recent electrochemical experiments revealed a linear dependence of the $Ni^{II/I}$ reduction potential on pH with a slope of 57 mV/pH unit, implicating a proton-coupled electron transfer (PCET) process with the same number of electrons and protons transferred. The combined theoretical and experimental studies herein provide an explanation for this pH dependence in the context of the overall proposed catalytic mechanism. In the proposed mechanisms, the catalytic cycle begins with a series of intermolecular proton transfers from an acid to the pendant amine ligand and electrochemical electron transfers to the nickel center to produce the doubly protonated Ni^0 species, a precursor to H_2 evolution. The calculated $Ni^{II/I}$ reduction potentials of the doubly protonated species are in excellent agreement with the experimentally observed reduction potential in the presence of strong acid, suggesting that the catalytically active species leading to the peak observed in these cyclic voltammetry (CV) experiments is doubly protonated. The $Ni^{I/0}$ reduction potential was found to be slightly more positive than the $Ni^{II/I}$ reduction potential, indicating that the $Ni^{I/0}$ reduction occurs spontaneously after the $Ni^{II/I}$ reduction, as implied by the experimental observation of a single CV peak. These results suggest that the PCET process observed in the CV experiments is a two-electron/two-proton process corresponding to an initial double protonation followed by two reductions. On the basis of the experimental and theoretical data, the complete thermodynamic scheme and the Pourbaix diagram were generated for this catalyst. The Pourbaix diagram, which identifies the most thermodynamically stable species at each reduction potential and pH value, illustrates that this catalyst undergoes different types of PCET processes for various pH ranges. These thermodynamic insights will aid in the design of more effective molecular catalysts for H_2 production.

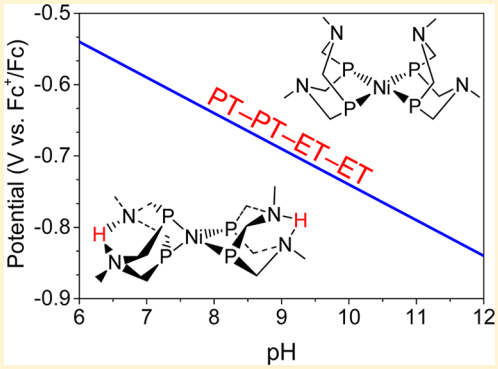

INTRODUCTION

Efficient generation and subsequent storage of energy from renewable resources continues to be an important area of research.[1,2] A promising direction is the use of H_2 in fuel cells and other energy devices.[3] Such processes require cost-effective, man-made, mass-produced catalysts directed toward H_2 oxidation and evolution.[2,3] Current industrial catalysts contain costly platinum, making them impractical for large-scale production.[4] On the other hand, hydrogen oxidation and production are catalyzed in nature by hydrogenase enzymes,[5] which serve as inspiration for the design of molecular catalysts. Examples of such catalysts are the Ni-based $P_2^RN_2^{R'}$ electrocatalysts,[6−8] which were designed to mimic the pendant amine ligands found in hydrogenase enzymes. Here $P_2^RN_2^{R'}$ denotes 1,5-R′-diaza-3,7-R-diphosphacyclooctane ligands with substituents R and R′ covalently bound to P and N, respectively. These molecular electrocatalysts contain phosphorus in the first coordination sphere of the metal and nitrogen in the second coordination sphere. The nitrogen atoms act as proton relays, transferring protons intramolecularly to and from the Ni center and intermolecularly to and from species in solution. Depending on the R and R′ substituents, these complexes can catalyze either H_2 oxidation or production. These catalysts have been studied extensively with experimental and theoretical methods.[6−24]

Received: September 21, 2012
Published: March 11, 2013

   dx.doi.org/10.1021/ic302056j | Inorg. Chem. 2013, 52, 3643−3652

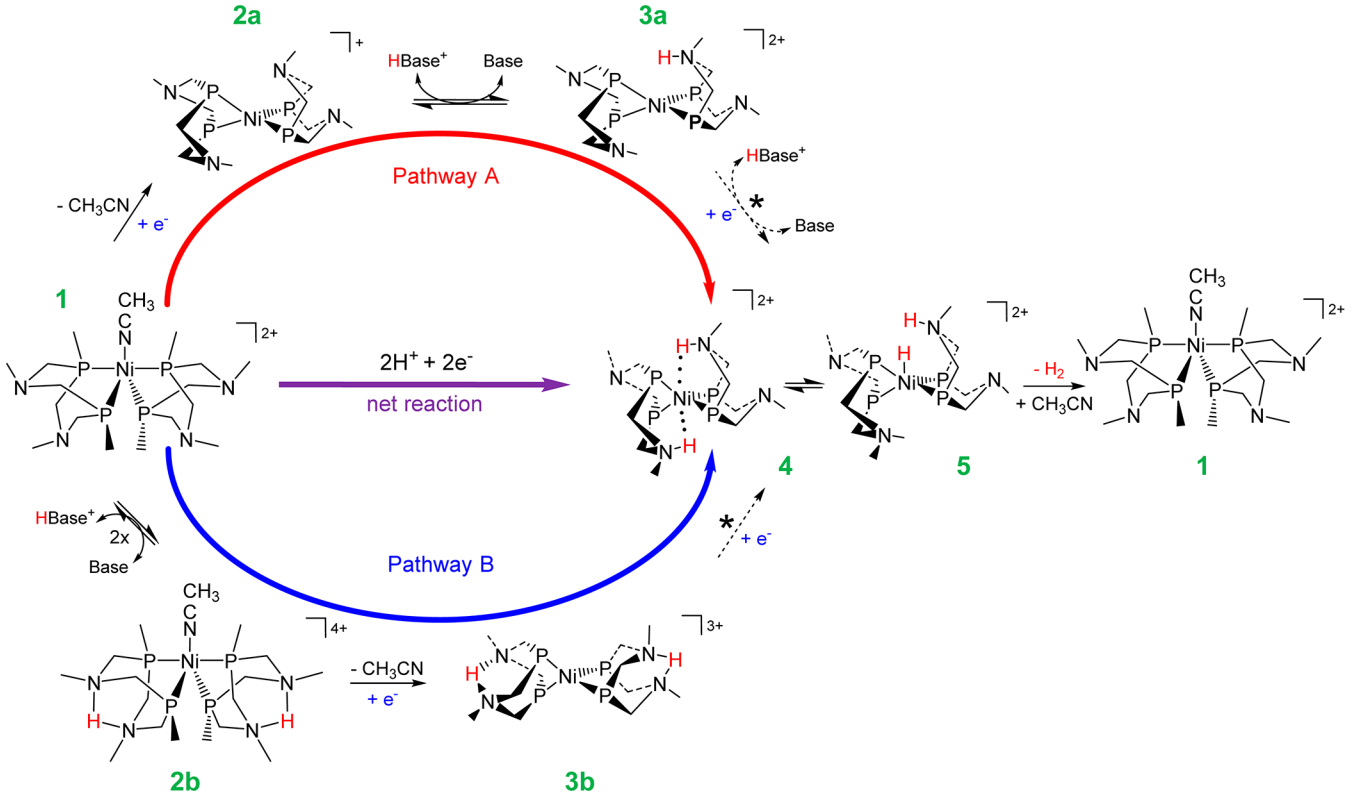

Figure 1. Proposed mechanisms for H_2 production involving a series of electron and proton transfer steps. Pathway A (red) is characterized by an initial reduction (**2a**), followed by intermolecular proton transfer (**3a**). Pathway B (blue) is characterized by an initial double intermolecular proton transfer (**2b**), followed by a reduction (**3b**). The dashed arrows indicate a net transfer of one electron and one proton for Pathway A and one electron for Pathway B. The asterisk by each dashed arrow indicates that the system is thought to undergo one or more of the following: ring isomerization, intramolecular proton transfer, and intermolecular proton transfer. The alternative Pathway A′ is the same as Pathway A except the first proton transfer occurs prior to the first reduction. The full substituents on P and N are not shown for clarity, and in species **2b** and **3b**, the proton is thought to be shared equally between the two nitrogens.

Recently, the effect of acid strength was investigated for the production of H_2 using $[Ni(P^{Ph}_2N^{Bn}_2)_2]^{2+}$ as a catalyst (Ph = phenyl; Bn = benzyl).[16] These electrochemical experiments indicated that the reduction potential of the $Ni^{II/I}$ couple shifted to values positive of the unprotonated $Ni^{II/I}$ couple under acidic conditions, where the largest shifts were observed with the strongest acids.[16] Measurement of the reduction potentials for several acids in acetonitrile (MeCN) revealed a linear relationship between the reduction potential and pH, as determined by the acid pK_a, with a slope of 57 mV/pH unit.[16] Such shifts are indicative of coupling between the protons and electrons via proton-coupled electron transfer (PCET). The main unanswered question from this experimental study is the fundamental nature of this coupling in the context of the overall mechanism for H_2 evolution.

The net reaction of the catalytic cycle for hydrogen production is $2H^+ + 2e^- \rightarrow H_2$. Using the form of the Nernst equation for PCET reactions, the slope of the pH-dependence of the reduction potential is (m/n) 59 mV/pH unit for the transfer of n electrons and m protons at 298 K.[16,25−27] Thus, a one-electron/one-proton coupled process would give the same slope as a two-electron/two-proton coupled process. In the context of electrocatalytic H_2 production, both types of PCET processes would be consistent with the experimentally measured slope. The experimental data indicate that both singly and doubly protonated species may form, but the experiments do not enable the determination as to whether these species are stable yet unproductive intermediates or directly relevant to the catalytic cycle.[16] A wide range of mechanisms involving various electron transfer (ET) and proton transfer (PT) steps is possible.

Two proposed mechanisms for H_2 production are depicted in Figure 1, where the pathways for the first portion of the cycle are labeled as Pathway A (red) and Pathway B (blue). Pathway A begins with electrochemical reduction, leading to species **2a**, followed by intermolecular PT, leading to species **3a**, comprising a net reaction of $[Ni^{II}N]^{2+} + e^- + H^+ \rightarrow [Ni^{I}NH]^{2+}$. Subsequently, another electrochemical reduction and intermolecular PT occur to produce the doubly protonated Ni^0 species **4**. Pathway B begins with two intermolecular PT steps, leading to species **2b**, followed by two electrochemical reduction steps, leading to species **3b** and then to species **4**, comprising a net reaction of $[Ni^{II}N]^{2+} + 2e^- + 2H^+ \rightarrow [Ni^{0}NH_2]^{2+}$. For both pathways, the electrons are provided by the electrode, and the protons are provided by acid molecules in solution. Based on previous experimental and theoretical studies, the later steps leading to species **4** are thought to involve one or more of the following: ring isomerization, intramolecular PT between the Ni center and the pendant amine, and intermolecular PT between the acid/base in solution and the pendant amine. Because of the short lifetimes of the many possible intermediates relative to the experimentally accessible time scale, these steps are represented by dashed arrows with asterisks in Figure 1. The dashed arrows indicate a net transfer of one electron and one proton for Pathway A and one electron for Pathway B. Although Figure 1

dx.doi.org/10.1021/ic302056j | Inorg. Chem. 2013, 52, 3643−3652

depicts only sequential mechanisms, some ET and PT steps could occur via concerted mechanisms.[28−38] Distinguishing between sequential and concerted mechanisms is beyond the scope of this work.

To assist in interpreting the electrochemical experiments, we examined three different sequential pathways using a thermodynamic analysis. The first part of Pathway B (species **1** to **3b**) is presumed to occur via the PT−PT−ET mechanism shown in Figure 1 for reasons that will be explained below. While the first part of Pathway A (species **1** to **3a**) is shown to occur via an ET−PT mechanism in Figure 1, it could also occur with the proton transferring first via a PT−ET mechanism. The possibility of this alternative mechanism, denoted Pathway A′, will also be considered. To investigate these three pathways, we calculated the reduction potentials and the free energy differences for the various species occurring in the proposed mechanisms. An analysis of these calculations, as well as the experimental data, provides mechanistic insight into the experimentally observed pH dependence of the experimental cyclic voltammograms (CVs).

METHODS

We used density functional theory (DFT) with a dielectric continuum solvent model to calculate reduction potentials for comparison to available experimental electrochemical data. We also calculated reaction free energies to evaluate the different protonation pathways and to determine the viability of acid association before and after reduction of the Ni center. The reaction free energies, ΔG^0, were obtained from the differences in the free energies of the optimized solvated reactant and product structures. For notational simplicity, the $P_2^RN_2^{R'}$ catalyst is abbreviated (R,R′) for the remainder of the paper, and this work focuses on the $P_2^{Ph}N_2^{Bn}$ catalyst, abbreviated (Ph,Bn).

To examine the possible mechanisms, we calculated the reduction potentials of various protonated forms of the catalyst. We considered the singly protonated *endo* and *exo* forms, as well as the doubly protonated *endo*−*endo* and *exo*−*exo* forms, depicted in Figure 2. Each

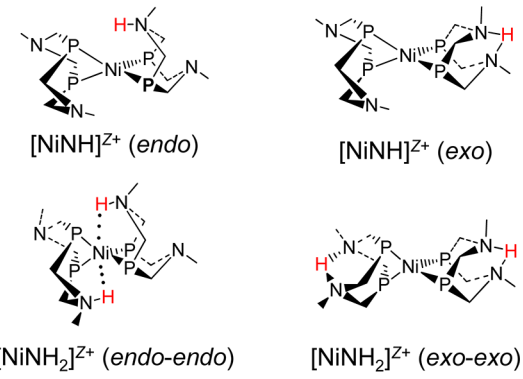

Figure 2. Relevant isomers of singly and doubly protonated forms of the Ni catalyst with charge +*Z*. The full substituents on P and N are not shown for clarity, and in *exo* and *exo*−*exo* species, the proton is thought to be shared equally between the two nitrogens.

protonated cyclic ligand of the Ni complex can be either *endo* or *exo* with respect to the metal center, corresponding to the six-membered chelate ring of the bidentate cyclic ligands arranged in either the boat or chair conformation, respectively. Note that for *exo* protonation, both chelate rings on that bidentate ligand are in the chair conformation, corresponding to the "pinched" configuration shown in Figure 2.

We also investigated the association of both weak and strong acids hydrogen bonded to the singly protonated catalyst in the *endo* conformation: *p*-anisidinium ($pK_a^{MeCN} \sim 11.9$, denoted "Asd") and *p*-cyanoanilinium ($pK_a^{MeCN} \sim 7.0$, denoted "Anl"), respectively.[16,39] In the acid−catalyst supramolecular complex, the amine substituent of the acid or conjugate base is hydrogen bonded to the pendant amine ligand of the Ni catalyst. For the associated acid−catalyst complexes, we examined four species corresponding to the four different charge transfer states with the electron and proton on their donors or acceptors. The two proton transfer states are denoted as either (NiN···HB), where the hydrogen bond is between the acid (HB) and the unprotonated Ni catalyst, or (NiNH···B), where the hydrogen bond is between the conjugate base (B) and the protonated Ni catalyst. The two electron transfer states correspond to the Ni^I and Ni^{II} oxidation states, respectively. These calculations enabled us to investigate the thermodynamics of proton transfer from the acid to the pendant amine of the catalyst both before and after reduction.

Computational Details. We calculated reduction potentials of the various species directly by optimizing the geometries in solution (MeCN). We also calculated the reduction potentials by applying the Born−Haber cycle with structures optimized in the gas phase for comparison.[40,41] Note that the use of structures optimized in the gas phase is not valid when large structural changes occur upon solvation. Based on the structural differences observed for some of the species optimized in the gas phase and in solution, we report only the solution-optimized data. For cases exhibiting minimal structural differences, the results of the two approaches were qualitatively similar (see Supporting Information). Selected bond distances and angles, as well as the Cartesian coordinates of the optimized structures, are available in the Supporting Information.

Detailed descriptions of the methods used to calculate reduction potentials were reported elsewhere,[21] and only a brief summary will be given here. All calculations were performed using the B3P86 density functional[42,43] in Gaussian 09.[44] We used the SDD pseudopotential and basis set of Preuss and co-workers for Ni,[45] the 6-31G** basis set for the protonated amine hydrogens of both acid and catalyst,[46] and the 6-31G* basis set for all other atoms.[47,48] A comparison to other functionals and basis sets is provided in the Supporting Information. We used the conductor-like polarizable continuum model (C-PCM)[49,50] with Bondi atomic radii[51] and included the nonelectrostatic interactions, specifically the dispersion,[52,53] repulsion,[52,53] and cavitation energies,[54] to obtain the solvent-optimized geometries.

To obtain the reduction potentials, standard relationships were used to cancel systematic error resulting from the chosen method and basis set.[21] Specifically, we used the following expression to calculate the $Ni^{II/I}$ reduction potentials of the singly and doubly protonated species:

$$E^0 = E^{0,\mathrm{ref}} - \Delta\Delta G_r^0(e^-)/F \quad (1)$$

In this expression, E^0 is the $Ni^{II/I}$ reduction potential for the species of interest; $E^{0,\mathrm{ref}}$ is the experimentally measured reduction potential of the reference species, which is the unprotonated (Ph,Bn) complex;[7,16] $\Delta\Delta G_r^0(e^-)$ is the calculated difference in free energies of the reduction reaction for the species of interest and the reference species; and *F* is Faraday's constant. In other words, the reduction potentials are calculated relative to the experimentally known $Ni^{II/I}$ reduction potential for the unprotonated (Ph,Bn) species. All calculated and experimental reduction potentials are given in volts (V) relative to the ferrocenium/ferrocene (Fc^+/Fc) couple in MeCN and are therefore directly comparable without the necessity of calculating the reduction potential for the Fc^+/Fc couple. Note that the calculated reduction potentials may be viewed as standard potentials that are relative to the Fc^+/Fc couple in acetonitrile and are calculated for various protonation states. The calculated value for the unprotonated species is assumed to be equal to the experimentally measured $E_{1/2}$ in the absence of acid. As discussed below, the calculated value for the doubly protonated species is shown to be consistent with the experimentally observed potential of the catalytic wave in the presence of the strongest acid.

The PT and association reaction free energies, ΔG_{PT}^0 and ΔG_{assoc}^0, respectively, are the free energy differences between the solvent-optimized structures. In the calculation of ΔG_{assoc}^0, we include the thermal contributions from the vibrations and translations but not

dx.doi.org/10.1021/ic302056j | Inorg. Chem. 2013, 52, 3643−3652

from the rotations for reasons discussed in ref 55 and summarized in the Supporting Information. The association reaction free energies calculated using various approaches are also provided in the Supporting Information. Moreover, ΔG^0_{assoc} does not account for basis set superposition error (BSSE). The BSSE could not be determined for the solvent-optimized structures, but gas-phase counterpoise-corrected calculations of these structures suggest that these errors would be small in this case. Lastly, we examined the acid−catalyst proton transfer reactions by calculating the one-dimensional proton potentials, where the coordinates of all nuclei except the transferring hydrogen were fixed. Although the three-dimensional analogues of these proton potentials could be generated, the qualitative trends are expected to be captured with the one-dimensional treatment of the proton motion. The technical details of these types of calculations were presented previously.[21,56]

RESULTS AND DISCUSSION

We investigated the singly and doubly protonated forms of the catalyst. While the singly protonated *endo* species has not been directly observed experimentally, at least one of the four protonated chelate rings must be in the *endo* orientation for H_2 production to occur according to the proposed mechanisms in Figure 1.[9,23] In contrast, NMR spectroscopy data have provided strong evidence for the presence of the doubly protonated *exo*−*exo* species in solution.[16] For the present study, the NMR spectroscopy studies reported in ref 16 were repeated in the presence of electrolyte and are in quantitative agreement with the previous results. These new experimental results suggest that the doubly protonated *exo*−*exo* species is dominant under electrochemical conditions as well as standard NMR spectroscopy conditions. The details of the experimental methods for these studies are provided in the Supporting Information.

Chair−boat isomerization from the *exo* or *exo*−*exo* form to the catalytically active *endo* or *endo*−*endo* form is thought to be required before H_2 can be produced. The chair−boat isomerization barrier for the protonated species is on the order of 10−15 kcal/mol and thus constitutes a possible bottleneck in the catalytic cycle.[9,17,23] This bottleneck is presumed to result in the low concentrations of the *endo*−*endo* form (**4**) that could undergo intramolecular proton transfer to form the protonated Ni-hydride species (**5**) that is thought to exergonically evolve H_2.[7,15,16]

An explanation for the lack of experimental observation of the singly protonated *endo* Ni^{II} and Ni^0 species with NMR spectroscopy was provided by previous calculations on the related (Ph,Ph) H_2 production catalyst.[9,17,23] These calculations indicated that the singly protonated Ni^0 species is much less stable than the doubly protonated Ni^0 species.[23] Moreover, upon *endo* protonation of the Ni^I species to form **3a** in Figure 1, the system readily undergoes PCET with intramolecular PT to the Ni center,[9] yielding a monohydride species that is extremely stable and observed by NMR spectroscopy for both the (Ph,Ph) and (Ph,Bn) catalysts.[7] Furthermore, intermolecular proton transfer to an *exo* protonation site is less sterically hindered and therefore may be more favorable, although it would require subsequent isomerization to the catalytically active *endo* form. Based on these previous experimental and theoretical studies, we considered the singly protonated *endo* and *exo* and the doubly protonated *endo*−*endo* and *exo*−*exo* (Ph,Bn) catalysts in this paper.

Reduction Potentials of Singly and Doubly Protonated Species. The calculated reduction potentials for the species described in the previous subsection are presented in Table 1. Because the $Ni^{II/I}$ couple of the unprotonated (Ph,Bn) catalyst is used as the reference, all other reduction potentials are calculated relative to this value, which agrees exactly with the experimental $Ni^{II/I}$ reduction potential by construction. In the crystal structure of the (Ph,Bn) catalyst and in crystal structures for similar electrocatalysts, a weakly bound MeCN ligand is coordinated to the unprotonated Ni^{II} species (**1**).[6,7,13,16,57] In contrast, the Ni^0 crystal structures for similar electrocatalysts are four-coordinate without a solvent ligand.[13,57,58] From a qualitative perspective, five-coordinate Ni^{II} complexes with a weakly coordinating solvent ligand and four-coordinate Ni^0 complexes are expected to be stable according to the 18-electron rule for metal complexes, whereas five-coordinate Ni^I complexes with a solvent ligand are not expected to be stable, as they would be 19-electron complexes. Thus, typically these Ni^{II} species are assumed to be five-coordinate with a solvent ligand, whereas these Ni^I and Ni^0 species are assumed to be four-coordinate without a solvent ligand.

Table 1. Calculated $Ni^{II/I}$ Reduction Potentials of Relevant Catalytic Species[a]

species		$E^0(Ni^{II/I})$
$[NiN]^{2+b}$		−0.94
$[NiNH]^{3+}$	*endo*[c]	−0.79
$[NiNH]^{3+}$	*exo*[c]	−0.86
$[NiNH_2]^{4+}$	*endo*−*endo*[c]	−0.57
$[NiNH_2]^{4+}$	*exo*−*exo*[c]	−0.57

[a]V vs Fc^+/Fc couple in MeCN. [b]Reference reduction potential used in eq 1, so it agrees with experimental $E_{1/2}$ value by construction; (bbcc) conformer from ref 21. [c]Isomers of singly and doubly protonated forms of Ni catalyst shown in Figure 2.

Consistent with the above discussion, we explicitly include an MeCN ligand for the Ni^{II} species but not for the Ni^I species in our calculations. Note that the free energy of solvation for the MeCN ligand is not required in the calculation of the $Ni^{II/I}$ reduction potentials using eq 1 because it cancels in the calculation of the difference in free energies of the reduction reactions for the species of interest and the reference species.[59] The calculated $Ni^{II/I}$ reduction potentials are consistent with the experimental data only by accounting for the change in coordination number upon reduction. Other approaches that treat both oxidation states the same (i.e., both the Ni^I and Ni^{II} species with or without the fifth ligand) yield a qualitatively different interpretation of the pathways leading to H_2 production. The results from alternative treatments are provided in the Supporting Information. These results suggest that the MeCN binding strength is different for the unprotonated, singly protonated, and doubly protonated species. As a result, the effects of the MeCN ligand are not additive and do not cancel when the unprotonated species is chosen as the reference.

For simplicity, we considered only the high and low pH limits in our calculations of the reduction potentials. At high pH values, the catalyst is unprotonated, so the experimentally measured reduction potential would be the reduction potential of the unprotonated catalyst and represents the most negative value for the observed potential: −0.94 V vs Fc^+/Fc.[7,16] Conversely, at very low pH values, the majority of the catalyst is protonated, so the experimentally measured reduction potential would be the reduction of the protonated species and represents the least negative value for the observed potential. These two regimes correspond to the plateau regions (i.e., pH-

dx.doi.org/10.1021/ic302056j | Inorg. Chem. 2013, 52, 3643−3652

independent regimes) in the plot of reduction potential versus pH. For intermediate pH values, a mixture of protonated and unprotonated species is present in solution such that the observed reduction potential changes linearly with pH. The experimental results indicate that for the strongest acid studied (2,5-dichloranilinium, $pK_a^{MeCN} \sim 6.2$), the potential at half the maximum current was observed to be −0.58 V vs Fc^+/Fc.[16]

The theoretical methodology used in this study allows us to calculate the reduction potentials of various protonated forms of the catalyst, such as *endo*, *exo*, *endo*−*endo*, and *exo*−*exo*. As evident from Table 1, the calculated reduction potentials of the singly protonated species (both *endo* and *exo*) are significantly more negative relative to the observed potential of the catalytic wave in the presence of the strongest acid (−0.58 V vs Fc^+/Fc), while the calculated reduction potentials of the doubly protonated species are in excellent agreement with this experimental value.[16] These results suggest that the catalytically active species is doubly protonated rather than singly protonated because the reduction potentials for the doubly protonated, but not the singly protonated, species are consistent with the cyclic voltammetry experiments. This observation is also consistent with the NMR spectroscopy experiments indicating the prevalence of the doubly protonated *exo*−*exo* species in solution.[16]

Proton Transfer Reactions and Association Free Energies. We examined the hydrogen-bonded associated acid−catalyst complexes with both a weak and a strong acid. The proton is transferring between the acid and the pendant amine of the catalyst, and the two proton transfer states of interest correspond to the proton on the acid or the catalyst. For electrochemical reactions, the electron is transferring between the complex and the electrode, so the two electron transfer states of interest correspond to the two oxidation states of the complex. For complexes with the weak acid, we found four stationary points corresponding to the four combinations of the electron and proton being on their donors and acceptors. For complexes with the strong acid, however, we were unable to determine stationary points with the proton on its donor (i.e., on the acid) but were able to identify two stationary points with the proton on its acceptor (i.e., on the catalyst pendant amine).

For the weak acid-associated complexes, we calculated the reaction free energies for the proton transfer steps in the ET−PT and PT−ET mechanisms associated with Pathways A and A′, respectively. The reaction free energies for these two PT steps are −0.03 and −0.09 eV, respectively. We also calculated the one-dimensional proton potentials for the proton transfer steps of the weak acid-associated complexes. These results are provided in the Supporting Information. These proton potentials were generated by moving the proton along a one-dimensional axis with all other atoms fixed and thus provide only a qualitative indication of the proton potential for these specific equilibrium structures. For the weak acid, the proton potentials corresponding to the equilibrium structures with the proton bonded to the acid exhibit relatively low barriers, suggesting relatively facile PT without significant hydrogen tunneling effects. As mentioned above, for the strong acid, we were unable to find equilibrium structures with the proton on the acid, also suggesting facile PT from the acid to the catalyst. Thus, proton transfer is likely to be facile after the acid−catalyst complex is formed.

To investigate the free energy associated with the formation of the acid−catalyst complex, we calculated the free energies of association, ΔG^0_{assoc}, before and after reduction for the *endo* isomer. The results are reported in Table 2. In all cases, the

Table 2. Calculated Reaction Free Energies for Acid Association to Ni Catalyst[a]

	base (B)	
association reaction	*p*-anisidine[b]	*p*-cyanoaniline[b]
$[Ni^{II}N]^{2+} + [HB]^+ \rightarrow [Ni^{II}N\cdots HB]^{3+}$	0.75	n/a
$[Ni^{II}N]^{2+} + [HB]^+ \rightarrow [Ni^{II}NH\cdots B]^{3+}$	0.65	0.44
$[Ni^{I}N]^{+} + [HB]^+ \rightarrow [Ni^{I}N\cdots HB]^{2+}$	0.26	n/a
$[Ni^{I}N]^{+} + [HB]^+ \rightarrow [Ni^{I}NH\cdots B]^{2+}$	0.24	0.06

[a]Reaction free energies in units of eV. [b]Reaction free energy, ΔG^0_{assoc}, obtained from free energies of optimized solvated reactant and product structures in the *endo* form. ΔG^0_{assoc} does not account for basis set superposition error (BSSE) and does not include rotational contributions to the partition function.

effect of bringing two positively charged species in close proximity to one another is thermodynamically unfavorable, yielding small association constants. Although still somewhat unfavorable, the reaction free energies are smaller for the strong acid than for the weak acid and decrease significantly after reduction. Both of these observations are consistent with basic electrostatic arguments. As mentioned above, ΔG^0_{assoc} includes the translational contributions but excludes the rotational contributions to the partition functions and does not account for BSSE. As a result of these approximations, these values are expected to provide only a qualitative evaluation of the relative favorability of association. In other words, the trends are meaningful, but the absolute magnitudes are not quantitatively reliable.

In addition to the thermodynamic penalty of acid association, steric hindrance could be a key factor, especially for less accessible protonation sites within the catalyst.[9,17,23] Note that acid−catalyst association may be more favorable for the *exo* isomer than for the *endo* isomer due to less steric hindrance. In this case, however, the complex must surmount a substantial free energy barrier for isomerization from the *exo* to the *endo* form. Moreover, while the acids examined here are typical of those studied experimentally,[16] as the size of the acid or the R and R′ substituents on the catalyst increases, the acid−catalyst association constants may become prohibitively small, particularly for *endo* protonation. To overcome these problems, a catalytic amount of water could be added to act as a Grötthus-type proton shuttle. Experimental evidence has shown that addition of water significantly increases the observed catalytic turnover frequency.[16,60,61]

Thermodynamic Scheme. Previously a thermodynamic scheme for the (Ph,Bn) catalyst was reported on the basis of experimentally determined values.[16] Within this thermodynamic scheme, however, relations between some species were omitted because these species were not directly observable. Moreover, for some of these processes (shown as dashed arrows in Scheme 3 of ref 16), only average values associated with two consecutive ET or PT steps were determined. Utilizing the data presented herein, we report a completed thermodynamic scheme for the (Ph,Bn) catalyst in Figure 3. These species are still depicted in gray to illustrate that their relative thermodynamic stabilities are determined from an analysis of the calculations presented herein rather than from direct experimental measurement.

dx.doi.org/10.1021/ic302056j | Inorg. Chem. 2013, 52, 3643−3652

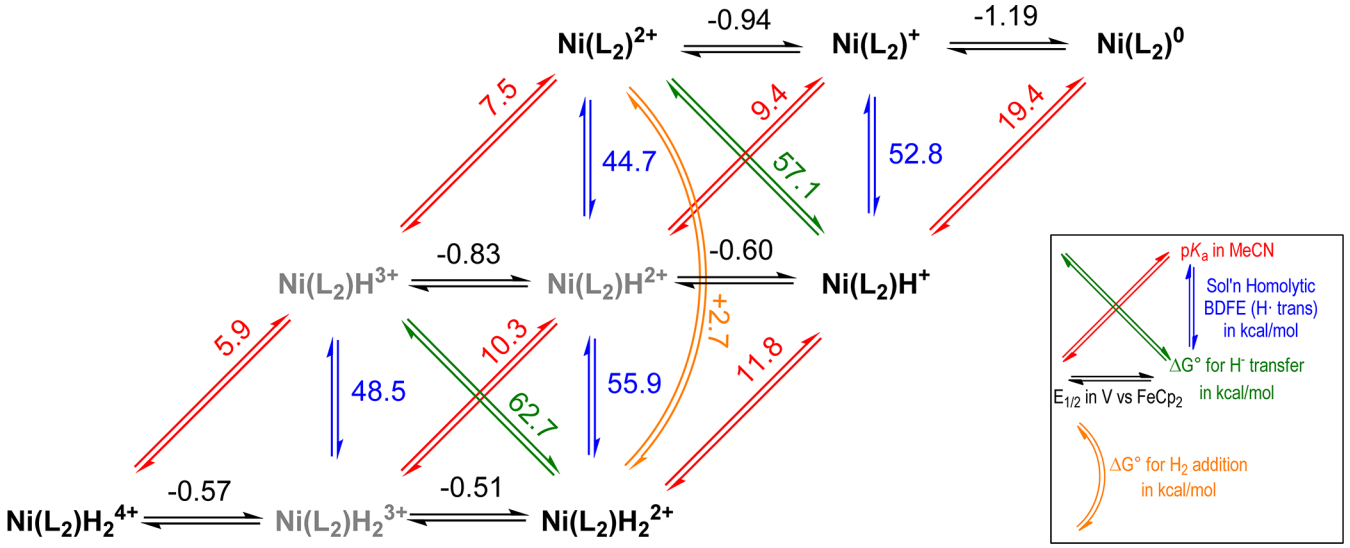

Figure 3. Experimental and calculated thermodynamic data for the (Ph,Bn) catalyst, where the P_2N_2 ligand is denoted by L. The thermodynamic scheme shows the relationships among the species in terms of $E_{1/2}$, pK_a, homolytic solution bond dissociation free energy (BDFE), $\Delta G^0_{H^-}$, and $\Delta G^0_{H_2}$ values. Formulas are intended to indicate only composition and not structure (i.e., notation does not distinguish between nickel hydrides and protonated pendant amines). The species in gray have not been directly observed experimentally, and their relative stabilities are therefore determined from the calculations presented herein. A version of this scheme was reported in ref 16; however, since all thermodynamic relationships have been determined, the scheme is presented here in its entirety. Details of the quantities required to complete this scheme are provided in the Supporting Information.

In ref 16 average values were reported for the double deprotonation of $[Ni^{II}NH_2]^{4+}$ to $[Ni^{II}N]^{2+}$ (left diagonal red arrows in Figure 3) and for the double reduction of $[Ni^{II}NH_2]^{4+}$ to $[Ni^{0}NH_2]^{2+}$ (lowest horizontal black arrows in Figure 3). Since these values are discussed herein, a summary of the methods used to obtain these average values is given. From previous ^{1}H and ^{31}P NMR spectroscopy studies, the relative ratios of acid/base and doubly protonated/unprotonated Ni^{II} (Ph,Bn) complex, respectively, were determined.[16] The equilibrium constant for the double deprotonation of $[Ni^{II}NH_2]^{4+}$ was calculated using the relative concentrations of the four species: $[Ni^{II}NH_2]^{4+} + 2[B] \rightleftharpoons [Ni^{II}N]^{2+} + 2[HB]^+$.[16] The equilibrium constant for this reaction (K_{eq}) was converted to an average pK_a value using the following expression: $pK_a^{MeCN,avg} = pK_a^{ref} - 0.5 \log(K_{eq})$, where pK_a^{ref} is the pK_a of the reference acid in acetonitrile (*p*-cyanoanilinium, $pK_a^{MeCN} \sim 7.0$).[16,39] As mentioned above, these results were reproduced in the presence of electrolyte, yielding an average pK_a of 6.8 ± 0.5, which is quantitatively similar to the previously measured value of 6.7 ± 0.4.[16] Note that the singly protonated complex was never observed in either set of experiments.

Using a combination of the experimentally determined average pK_a for $[Ni^{II}NH_2]^{4+}$ and the free energy for addition of H_2 to (Ph,Bn) of 2.7 kcal/mol,[7] the average potential for the double reduction of $[Ni^{II}NH_2]^{4+}$ to $[Ni^{0}NH_2]^{2+}$ can be determined using a thermodynamic cycle. As given in ref 16, this procedure leads to an average reduction potential of −0.54 V vs Fc^+/Fc. For complete details of the thermochemical reactions and relationships used to obtain this value, see the Supporting Information of ref 16. In addition to these average values, the shift in the reduction potential with acid strength was measured experimentally, and the following relationship was obtained from a linear fit of the pH-dependent reduction potential data:[16]

$$E = -0.057\ \text{V} \times \text{pH} - 0.230\ \text{V} \quad (2)$$

On the basis of the agreement between our calculated value for the $Ni^{II/I}$ reduction potential of the doubly protonated species and the experimental reduction potential at the lowest pH buffered solution studied, we deduce that the $Ni^{II/I}$ couple of $[Ni^{II}NH_2]^{4+}$ occurs at a potential of −0.57 V vs Fc^+/Fc (lower left black arrows in Figure 3). To obtain the average value of −0.54 V vs Fc^+/Fc discussed above, the $Ni^{I/0}$ couple of $[Ni^{I}NH_2]^{3+}$ must occur at a potential of −0.51 V vs Fc^+/Fc (lower right black arrows in Figure 3). Note that the second reduction (i.e., the $Ni^{I/0}$ couple) occurs at a potential positive of the first reduction (i.e., the $Ni^{II/I}$ couple) and as a result should occur spontaneously, most likely resulting from loss of the solvent ligand during the $Ni^{II/I}$ reduction. However, these values are considered to be virtually identical within the accuracy of the calculations. As given in Table 1, the $Ni^{II/I}$ reduction potentials of the singly protonated *endo* and *exo* $[Ni^{II}NH]^{3+}$ species are −0.79 and −0.86 V vs Fc^+/Fc, respectively. The difference between the reduction potentials of the *endo* and *exo* isomers for the singly protonated species is within the error of our calculations, and for this reason we utilize the average of these two potentials, −0.83 V vs Fc^+/Fc, for the $Ni^{II/I}$ reduction potential of $[Ni^{II}NH]^{3+}$ in Figure 3 (middle left black arrows) and the associated analysis.

A similar process can be used to obtain the pK_a values for the singly and doubly protonated Ni^{II} species. As discussed above, the experimental value of 6.7 is the average pK_a for the two protonation steps to form the *exo*−*exo* $[Ni^{II}NH_2]^{4+}$ species from the unprotonated Ni^{II} species. On the basis of the theoretical data, the reduction potential of the doubly protonated Ni^{II} species is −0.57 V vs Fc^+/Fc, and the experimentally obtained relation in eq 2 indicates that the pK_a of the doubly protonated species is 5.9 at this potential (lower left red arrows in Figure 3). To obtain an average pK_a of 6.7, the pK_a of the singly protonated Ni^{II} species must be 7.5 (upper left red arrows in Figure 3). In previous NMR spectroscopy experiments, the singly protonated Ni^{II} species

dx.doi.org/10.1021/ic302056j | Inorg. Chem. 2013, 52, 3643−3652

was not observed in equilibrium experiments using two different acids with pK_a values of 5.1 and 7.0,[16] suggesting that the pK_a of the singly protonated species is less than or equal to that of the doubly protonated species. While the experimental results suggest that the singly protonated species is less stable than the doubly protonated and unprotonated species in this pH range, the precise difference in energy is not indicated experimentally. Our calculations suggest that there may be a region of pH between 5.9 and 7.5 in which the singly protonated species is stable, but the pK_a values of 7.5 and 5.9 for the singly and doubly protonated Ni^{II} species are considered to be virtually identical within the accuracy of our calculations. Thus, this region may be narrower than calculated and therefore not experimentally observed, or it may not exist, given the limitations of the calculations. This issue does not impact the overall conclusions of the present work. For comparison, we generated a thermodynamic scheme using the average reduction potentials and average pK_a values for these steps and provide this alternative scheme in Figure S1 of the Supporting Information. The thermodynamic values in this alternative scheme are the same as those in Figure 3 to within the accuracy of the calculations and experiments.

Pourbaix Diagram. The linear fit of the experimental data[16] has a slope of 57 mV/pH unit (eq 2), which is similar to the slope of 59 mV/pH unit expected for a PCET process involving the same number of electrons and protons, as indicated by the standard form of the Nernst equation for PCET reactions.[25,27] Based on the agreement between the calculated and experimental reduction potentials, we deduced that the observed shift of the reduction potential in the presence of the strongest acid arises from the $Ni^{II/I}$ reduction of the doubly protonated species. Given the experimentally observed slope of ~59 mV/pH unit, as well as the lack of experimental observation of the singly protonated species, this PCET process is presumed to involve the transfer of two electrons, along with the transfer of two protons, on the time scale accessible in the CV experiments. According to this analysis, this PCET process connects species **1** and **4** through Pathway B in Figure 1. In other words, the PCET process observed in the CV experiments under catalytic conditions is the PT−PT−ET−ET process in Pathway B.

On the basis of the calculated data given in Table 1 and Figure 3, in conjunction with the experimental data reported in Figure 6 of ref 16, we generated the Pourbaix diagram for the (Ph,Bn) catalyst in MeCN. The resulting Pourbaix diagram,[62] which depicts the most thermodynamically stable species for a given reduction potential and pH value, is presented in Figure 4. In this figure, the horizontal and vertical black lines correspond to the reduction potentials and pK_a's, respectively, of various protonated and unprotonated forms of the (Ph,Bn) catalyst. The portions of the Pourbaix diagram at pH < 5 and pH > 20 are independent of acid concentration (horizontal black lines) and represent the reduction of the doubly protonated species ($2e^-$ process) and reduction of the unprotonated species (two $1e^-$ processes), respectively. In between these two limits of pH, various protonated forms of the catalyst are thermodynamically stable. The blue line between pH ≈ 8 and pH ≈ 12 has a slope consistent with the two-electron/two-proton ($2e^-$−$2H^+$) process shown in Pathway B of Figure 1 and corresponds to the experimentally measured slope reported in eq 2 from ref 16.

For other ranges of pH, the Pourbaix diagram has regions that correspond to different PCET processes that were not

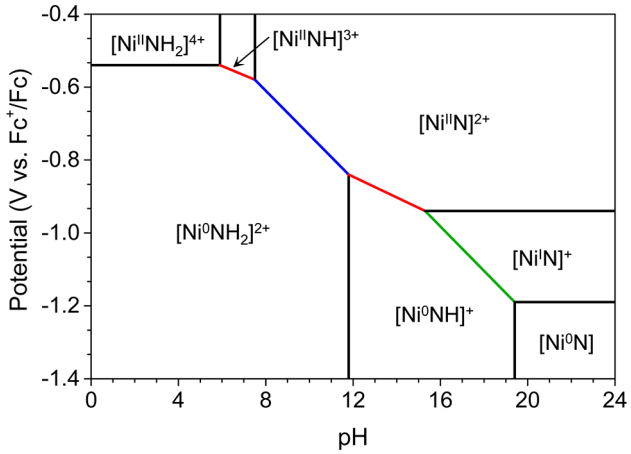

Figure 4. Pourbaix diagram[62] for the (Ph,Bn) catalyst calculated from the thermodynamic scheme in Figure 3. The horizontal and vertical lines are the reduction potentials and pK_a's, respectively, of various protonated and unprotonated forms of the catalyst in MeCN. The red lines have slopes of ~29.5 mV/pH unit and correspond to $2e^-$−$1H^+$ processes. The blue line has a slope of ~59 mV/pH unit and corresponds to a $2e^-$−$2H^+$ process. The green line has a slope of ~59 mV/pH unit and corresponds to a $1e^-$−$1H^+$ process. The analogous Pourbaix diagram that does not include the $[Ni^{II}NH]^{3+}$ region is provided as Figure S2 in the Supporting Information. Note that $[Ni^0NH]^+$ corresponds to the Ni^{II}-hydride species.

studied experimentally. The green line between pH ≈ 15 and pH ≈ 20 has a slope consistent with a $1e^-$−$1H^+$ process and corresponds to conversion between the $[Ni^0NH]^+$ species and the unprotonated Ni^I species. Because the same number of electrons and protons are being transferred, the green line ($1e^-$−$1H^+$ process) has the same slope of ~59 mV/pH unit as the blue line ($2e^-$−$2H^+$ process). The red line between pH ≈ 12 and pH ≈ 15 has a slope consistent with a $2e^-$−$1H^+$ process and corresponds to conversion between the $[Ni^0NH]^+$ species and the unprotonated Ni^{II} species. Note that $[Ni^0NH]^+$ corresponds to the Ni^{II}-hydride species rather than the singly protonated amine Ni^0 species. Thus, the red line is bounded on the left by the pK_a of 11.8 for the doubly protonated Ni^0 species (i.e., removal of a proton from the pendant amine as well as intramolecular proton transfer from the other pendant amine to the Ni center), and the green line is bounded on the right by the pK_a of 19.4 for the Ni^{II}-hydride species (i.e., removal of a proton from the metal center), as reported in Figure 3.

In addition to the $2e^-$−$1H^+$ process between pH ≈ 12 and pH ≈ 15, a second red line between pH ≈ 6 and pH ≈ 8 also has a slope consistent with a $2e^-$−$1H^+$ process, corresponding to conversion between the doubly protonated Ni^0 species and the singly protonated Ni^{II} species. This red line is bounded by the two pK_a values of the doubly and singly protonated Ni^{II} species, 5.9 and 7.5, respectively, as reported in Figure 3. As discussed above, the singly protonated species is not observed in the experiments. Moreover, the differences in these pK_a values (5.9 and 7.5) are within the errors of our calculations, and this region may be narrower than calculated or may not exist. For this reason, we also present an alternative version of Figure 4 in Figure S2 of the Supporting Information using the average pK_a value for these steps, as well as the average reduction potential for the doubly protonated Ni^{II} and Ni^I species. The only difference between Figure 4 and Figure S2 is that the area associated with the singly protonated species disappears, and only the doubly protonated Ni^{II} species is

dx.doi.org/10.1021/ic302056j | Inorg. Chem. 2013, 52, 3643−3652

shown for pH values lower than ∼7 in Figure S2. This difference does not affect the overall conclusions of this paper. A description of the approach used to generate these Pourbaix diagrams, as well as the specific reduction potentials and pK_a's, are also provided in the Supporting Information.

H_2 Production Mechanism: Effects of Acid Strength. Our calculated reduction potential for the doubly protonated species is consistent with the experimentally observed potential for the catalytic wave in the presence of the strongest acid, suggesting that the doubly protonated species is being reduced in these CV experiments.[16] The linear fit of the experimental pH dependence follows the standard form of the Nernst equation for PCET reactions.[25,27] Thus, the combination of theoretical and experimental data implies that the pH dependence can be explained in the context of this Nernst equation, where the catalyst is present in a mixture of unprotonated and doubly protonated forms. For the strongest acids studied (pK_a's less than ∼7), the doubly protonated form dominates, and H_2 production occurs mainly through Pathway B with a reduction potential near −0.58 V vs Fc^+/Fc. For very weak acids (pK_a's greater than ∼12), the unprotonated form dominates, and H_2 production occurs mainly through Pathway A with a reduction potential near −0.94 V vs Fc^+/Fc, the value for the unprotonated catalyst. For intermediate strength acids (blue lines in Figures 4 and S2), a mixture of unprotonated and doubly protonated forms is present, and H_2 production occurs through both Pathways A and B, where the reduction potential is controlled by the relative populations of the unprotonated and doubly protonated forms.

We also considered an alternative explanation of the pH dependence. In a sequential PCET process, protonation could occur either before or after electron transfer. Protonation prior to reduction could result in a very large shift in potential because the electron is transferred to chemically distinct species, as in Pathway A′ and Pathway B. The above analysis of the pH dependence is based on this effect. However, protonation after reduction can also significantly affect the observed reduction potential if the PT reaction is fast and exergonic. This scenario could be relevant to Pathway A. To estimate the magnitude of the shift in potential that may occur due to a subsequent PT reaction, digital simulations of this process were performed, as described in detail in the Supporting Information. For a diffusion-controlled, second-order reaction (catalyst plus one substrate) that is exergonic, the maximum shift in potential is estimated to be ∼270 mV under conditions similar to those reported for the currently discussed catalytic process. For processes that are slower than diffusion controlled, the shift in potential will be even smaller, and similarly, for processes with a higher reaction order, the shift in potential is also expected to be smaller. Therefore, a fast subsequent PT reaction does not appear to provide a suitable explanation for the entirety of the previously observed shift in potential of up to 440 mV.[16] This type of kinetic potential shift could explain the pH dependence of the reduction potential for weak acids but not the observed shifts for the strongest acids, although this effect may contribute at some level to the overall observed pH dependence.

The experimentally measured catalytic rate in the regime independent of acid concentration was observed to increase with increasing pH.[16] In particular, the rate with *p*-anisidinium, the weakest acid studied, is much larger than the rates for the stronger acids. One possible explanation for this behavior is that the mechanism is predominantly Pathway A rather than Pathway B for *p*-anisidinium due to the higher population of the unprotonated form of the catalyst. Pathway A may require fewer isomerizations, which are thought to be rate determining in the overall catalytic cycle. Another possible explanation for this behavior is that the difference in pK_a values between the *p*-anisidinium (pK_a^{MeCN} ∼ 11.9) and the doubly protonated Ni^0 catalyst (pK_a^{MeCN} = 11.8)[7,16] is smallest for *p*-anisidinium, resulting in more facile deprotonation and reprotonation of the amine groups on the catalyst. As a result of this pK_a matching, the isomerization reactions are expected to be faster, and therefore would be less of a hindrance if they are required during the catalytic cycle. Both factors may contribute to the higher rate observed using *p*-anisidinium.

The net reaction for H_2 production requires two reduction steps, as illustrated in Figure 1. In this paper, we calculated the reduction potential for only the first reduction step, but we also consider these results in the context of the overall catalytic cycle by analyzing the thermodynamic scheme. For Pathway A (ET−PT mechanism), the $Ni^{II/I}$ reduction potential of the unprotonated species is −0.94 V vs Fc^+/Fc,[7,16] whereas for Pathway A′ (PT−ET mechanism), the $Ni^{II/I}$ reduction potential of the singly protonated species (average of the two isomers) is −0.83 V vs Fc^+/Fc. For Pathway B, the $Ni^{II/I}$ reduction potential for the doubly protonated species is −0.57 V vs Fc^+/Fc. If Pathways A and A′ follow a PT−ET mechanism for the later part of the cycle (dashed arrows in Figure 1), all three pathways contain some combination of two PT reactions and an ET reaction prior to the second ET reaction. For the resulting doubly protonated Ni^I species, the subsequent $Ni^{I/0}$ reduction occurs at a more positive potential of −0.51 V vs Fc^+/Fc and should occur spontaneously, most likely due to the solvent ligand release occurring during the $Ni^{II/I}$ reduction. If Pathways A and A′ follow an ET−PT mechanism for the later part of the cycle instead, the subsequent $Ni^{I/0}$ reduction of the singly protonated Ni^I species still occurs at a more positive potential of −0.60 V vs Fc^+/Fc and should also occur spontaneously, as it is positive of the $Ni^{II/I}$ couple for the singly protonated species.

Thus, regardless of the pathway, the experimentally observed reduction potential arises from the $Ni^{II/I}$ couple, and the subsequent $Ni^{I/0}$ reduction occurs spontaneously. These results are consistent with the experimental observation of only a single peak in the CV.[16] This analysis illustrates that a combination of pathways is possible, and the branching among these pathways is likely pH-dependent.[16] For all pathways, a series of isomerizations and deprotonations/protonations most likely occur prior to and/or subsequent to the second reduction step, and the barriers to these processes may be prohibitively large and rate-determining.[9,17,23] We emphasize that this type of thermodynamic analysis can be used to rule out certain mechanisms and can be found to be consistent with proposed mechanisms but cannot unequivocally prove a particular mechanism.

■ CONCLUSIONS

In this paper, we investigated three proposed mechanisms for H_2 evolution catalyzed by the $[Ni(P^{Ph}_2N^{Bn}_2)_2]^{2+}$ molecular electrocatalyst. The net reaction of the catalytic cycle for hydrogen production is $2H^+ + 2e^- \rightarrow H_2$. The electrons are provided by the electrode, and the protons are provided by acid molecules in solution. Pathway A is characterized by an initial reduction, followed by intermolecular proton transfer (ET−PT), whereas Pathway A′ occurs in the reverse order (PT−

dx.doi.org/10.1021/ic302056j | Inorg. Chem. 2013, 52, 3643−3652

ET). Both of these pathways are followed by an additional reduction and proton transfer in an unspecified order. Pathway B is characterized by an initial double intermolecular proton transfer, followed by two reductions (PT−PT−ET−ET). All three pathways converge at the doubly protonated Ni^0 species, a precursor to H_2 evolution. The reduction potentials and relative free energies of the singly and doubly protonated species along these reaction pathways were calculated to identify the pathway that is most consistent with the experimental data.

The experimentally observed slope of the pH-dependence of the $Ni^{II/I}$ reduction potential is consistent with the slope of 59 mV/pH unit predicted by the Nernst equation for PCET reactions with the same number of electrons and protons transferred.[25,27] The calculated $Ni^{II/I}$ reduction potentials of the doubly protonated species are in excellent agreement with the experimentally observed reduction potential in the presence of strong acid, suggesting that the catalytically active species leading to the peak observed in these CV experiments is doubly protonated. This observation is also consistent with the NMR spectroscopy experiments implicating the prevalence of the doubly protonated *exo*−*exo* species in solution.[16] The second $Ni^{I/0}$ reduction potential was found to be slightly more positive than the initial $Ni^{II/I}$ reduction potential, indicating that the $Ni^{I/0}$ reduction occurs spontaneously, as implied by the experimental observation of a single CV peak. The more positive reduction potential for the $Ni^{I/0}$ reduction could arise from the solvent ligand release occurring during the $Ni^{II/I}$ reduction. On the basis of the experimentally observed slope of the pH-dependence of the reduction potential, in conjunction with the calculated reduction potentials, the PCET process observed in the CV experiments with strong acid was deduced to be consistent with the two-electron/two-proton process corresponding to an initial double protonation followed by two reductions.

Utilizing a combination of experimental and calculated data, we completed the previously underdetermined thermodynamic scheme for the (Ph,Bn) catalyst.[16] Moreover, we generated the Pourbaix diagram for this catalyst to identify the most thermodynamically stable species at each reduction potential and pH value for a wide range of pH values. The Pourbaix diagram illustrates that the (Ph,Bn) catalyst undergoes several different types of PCET processes, including one-electron/one-proton and two-electron/one-proton processes, as well as the two-electron/two-proton process observed in the CV experiments between pH ≈ 7 and pH ≈ 12.[16]

Although important information can be gained by examining the different ET and PT steps along the catalytic cycle, these types of studies do not provide complete knowledge about the effectiveness of specific catalysts. In this paper, we have focused on the thermodynamic aspects of catalysis and have not examined the kinetic aspects, which would require the calculation of barriers along the various mechanistic pathways. Furthermore, for situations in which these catalysts must work reversibly, the barriers in the reverse direction must also be analyzed. In general, all possible steps along the catalytic cycle must be investigated under the appropriate experimental conditions to aid in the design of more effective nickel-based molecular electrocatalysts.

■ ASSOCIATED CONTENT

Supporting Information

Description of computational methods; selected geometric parameters and Cartesian coordinates of solution-phase optimized structures; $Ni^{II/I}$ reduction potentials calculated using different approaches; association reaction free energies calculated using different approaches; relative energies of protonated species using alternate approaches; one-dimensional proton potentials for acid−catalyst complexes with weak acid; description of experimental methods and results; alternative thermodynamic scheme and Pourbaix diagram; table of related hydrogen reaction free energies in MeCN. This material is available free of charge via the Internet at http://pubs.acs.org.

■ AUTHOR INFORMATION

Corresponding Author

*E-mail: shs3@illinois.edu.

Notes

The authors declare no competing financial interest.

■ ACKNOWLEDGMENTS

We thank Brian Solis, Alexander Soudackov, Monte Helm, Shentan Chen, and Simone Raugei for their helpful scientific discussions and insights. We would especially like to thank Wendy Shaw, Ming-Hsun Ho, and Roger Rousseau for their assistance with the Pourbaix diagrams. This research was supported as part of the Center for Molecular Electrocatalysis, an Energy Frontier Research Center funded by the U.S. Department of Energy, Office of Science, Office of Basic Energy Sciences.

■ REFERENCES

(1) McEvoy, J. P.; Brudvig, G. W. *Chem. Rev.* **2006**, *106*, 4455−4483.
(2) Savéant, J.-M. *Chem. Rev.* **2008**, *108*, 2348−2378.
(3) Lubitz, W.; Tumas, W. *Chem. Rev.* **2007**, *107*, 3900−3903 and references contained within this special issue.
(4) Ralph, T. R.; Hogarth, M. P. *Platinum Met. Rev.* **2002**, *46*, 117−135.
(5) Tard, C.; Pickett, C. J. *Chem. Rev.* **2009**, *109*, 2245−2274.
(6) Wilson, A. D.; Newell, R. H.; McNevin, M. J.; Muckerman, J. T.; Rakowski DuBois, M.; DuBois, D. L. *J. Am. Chem. Soc.* **2006**, *128*, 358−366.
(7) Fraze, K.; Wilson, A. D.; Appel, A. M.; Rakowski DuBois, M.; DuBois, D. L. *Organometallics* **2007**, *26*, 3918−3924.
(8) Wilson, A. D.; Shoemaker, R. K.; Miedaner, A.; Muckerman, J. T.; DuBois, D. L.; Rakowski DuBois, M. *Proc. Natl. Acad. Sci. U.S.A.* **2007**, *104*, 6951−6956.
(9) Raugei, S.; Chen, S.; Ho, M.-H.; Ginovska-Pangovska, B.; Rousseau, R. J.; Dupuis, M.; DuBois, D. L.; Bullock, R. M. *Chem.—Eur. J.* **2012**, *18*, 6493−6506.
(10) Wiese, S.; Kilgore, U. J.; DuBois, D. L.; Bullock, R. M. *ACS Catal.* **2012**, *2*, 720−727.
(11) Pool, D. H.; Stewart, M. P.; O'Hagan, M.; Shaw, W. J.; Roberts, J. A. S.; Bullock, R. M.; DuBois, D. L. *Proc. Natl. Acad. Sci. U.S.A.* **2012**, *109*, 15634−15639.
(12) Smith, S. E.; Yang, J. Y.; DuBois, D. L.; Bullock, R. M. *Angew. Chem., Int. Ed.* **2012**, *51*, 3152−3155.
(13) Wiedner, E. S.; Yang, J. Y.; Chen, S.; Raugei, S.; Dougherty, W. G.; Kassel, W. S.; Helm, M. L.; Bullock, R. M.; Rakowski DuBois, M.; DuBois, D. L. *Organometallics* **2012**, *31*, 144−156.
(14) DuBois, D. L.; Bullock, R. M. *Eur. J. Inorg. Chem.* **2011**, 1017−1027.
(15) Yang, J. Y.; Bullock, R. M.; Rakowski DuBois, M.; DuBois, D. L. *MRS Bull.* **2011**, *36*, 39−47.

(16) Appel, A. M.; Pool, D. H.; O'Hagan, M.; Shaw, W. J.; Yang, J. Y.; Rakowski DuBois, M.; DuBois, D. L.; Bullock, R. M. *ACS Catal.* **2011**, *1*, 777−785.
(17) O'Hagan, M.; Shaw, W. J.; Raugei, S.; Chen, S.; Yang, J. Y.; Kilgore, U. J.; DuBois, D. L.; Bullock, R. M. *J. Am. Chem. Soc.* **2011**, *133*, 14301−14312.
(18) Small, Y. A.; DuBois, D. L.; Fujita, E.; Muckerman, J. T. *Energy Environ. Sci.* **2011**, *4*, 3008−3020.
(19) Rakowski DuBois, M.; DuBois, D. L. *Chem. Soc. Rev.* **2009**, *38*, 62−72.
(20) Rakowski Dubois, M.; Dubois, D. L. *Acc. Chem. Res.* **2009**, *42*, 1974−1982.
(21) Fernandez, L. E.; Horvath, S.; Hammes-Schiffer, S. *J. Phys. Chem. C* **2012**, *116*, 3171−3180.
(22) Horvath, S.; Fernandez, L. E.; Soudackov, A. V.; Hammes-Schiffer, S. *Proc. Natl. Acad. Sci. U.S.A.* **2012**, *109*, 15663−15668.
(23) O'Hagan, M.; Ho, M.-H.; Yang, J. Y.; Appel, A. M.; Rakowski DuBois, M.; Raugei, S.; Shaw, W. J.; DuBois, D. L.; Bullock, R. M. *J. Am. Chem. Soc.* **2012**, *134*, 19409−19424.
(24) Fernandez, L. E.; Horvath, S.; Hammes-Schiffer, S. *J. Phys. Chem. Lett.* **2013**, *4*, 542−546.
(25) Slattery, S. J.; Blaho, J. K.; Lehnes, J.; Goldbsy, K. A. *Coord. Chem. Rev.* **1998**, *174*, 391−416.
(26) Bard, A. J.; Faulkner, L. R. *Electrochemical Methods: Fundamentals and Applications*, 2nd ed.; John Wiley & Sons, Inc.: New York, 2001.
(27) Savéant, J.-M. *Elements of Molecular and Biomolecular Electrochemistry: An Electrochemical Approach to Electron Transfer Chemistry*; Wiley-Interscience: Hoboken, NJ, 2006.
(28) Cukier, R. I.; Nocera, D. G. *Annu. Rev. Phys. Chem.* **1998**, *49*, 337−369.
(29) Soudackov, A.; Hammes-Schiffer, S. *J. Chem. Phys.* **1999**, *111*, 4672−4687.
(30) Hammes-Schiffer, S.; Soudackov, A. V. *J. Phys. Chem. B* **2008**, *112*, 14108−14123.
(31) Mayer, J. M. *Annu. Rev. Phys. Chem.* **2004**, *55*, 363−390.
(32) Huynh, M. H. V.; Meyer, T. J. *Chem. Rev.* **2007**, *107*, 5004−5064.
(33) Costentin, C. *Chem. Rev.* **2008**, *108*, 2145−2179.
(34) Costentin, C.; Robert, M.; Savéant, J.-M. *Chem. Rev.* **2010**, *110*, PR1−PR40.
(35) Hammes-Schiffer, S.; Stuchebrukhov, A. A. *Chem. Rev.* **2010**, *110*, 6939−6960.
(36) Costentin, C.; Robert, M.; Savéant, J.-M. *J. Am. Chem. Soc.* **2007**, *129*, 5870−5879 and references therein.
(37) Costentin, C.; Robert, M.; Savéant, J.-M. *J. Electroanal. Chem.* **2006**, *588*, 197−206.
(38) Warren, J. J.; Tronic, T. A.; Mayer, J. M. *Chem. Rev.* **2010**, *110*, 6961−7001.
(39) Kaljurand, I.; Kütt, A.; Sooväli, L.; Rodima, T.; Mäemets, V.; Leito, I.; Koppel, I. A. *J. Org. Chem.* **2005**, *70*, 1019−1028.
(40) Saracino, G. A. A.; Improta, R.; Barone, V. *Chem. Phys. Lett.* **2003**, *373*, 411−415.
(41) Roy, L. E.; Jakubikova, E.; Guthrie, M. G.; Batista, E. R. *J. Phys. Chem. A* **2009**, *113*, 6745−6750.
(42) Becke, A. D. *J. Chem. Phys.* **1993**, *98*, 5648−5652.
(43) Perdew, J. P. *Phys. Rev. B* **1986**, *33*, 8822−8824.
(44) Frisch, M. J.; Trucks, G. W.; Schlegel, H. B.; Scuseria, G. E.; Robb, M. A.; Cheeseman, J. R.; Scalmani, G.; Barone, V.; Mennucci, B.; Petersson, G. A.; Nakatsuji, H.; Caricato, M.; Li, X.; Hratchian, H. P.; Izmaylov, A. F.; Bloino, J.; Zheng, G.; Sonnenberg, J. L.; Hada, M.; Ehara, M.; Toyota, K.; Fukuda, R.; Hasegawa, J.; Ishida, M.; Nakajima, T.; Honda, Y.; Kitao, O.; Nakai, H.; Vreven, T.; Montgomery, J. J. A.; Peralta, J. E.; Ogliaro, F.; Bearpark, M.; Heyd, J. J.; Brothers, E.; Kudin, K. N.; Staroverov, V. N.; Kobayashi, R.; Normand, J.; Raghavachari, K.; Rendell, A.; Burant, J. C.; Iyengar, S. S.; Tomasi, J.; Cossi, M.; Rega, N.; Millam, N. J.; Klene, M.; Knox, J. E.; Cross, J. B.; Bakken, V.; Adamo, C.; Jaramillo, J.; Gomperts, R.; Stratmann, R. E.; Yazyev, O.; Austin, A. J.; Cammi, R.; Pomelli, C.; Ochterski, J. W.; Martin, R. L.; Morokuma, K.; Zakrzewski, V. G.; Voth, G. A.; Salvador, P.; Dannenberg, J. J.; Dapprich, S.; Daniels, A. D.; Farkas, Ö.; Foresman, J. B.; Ortiz, J. V.; Cioslowski, J.; Fox, D. J. *Gaussian 09, Revision B.01*; Gaussian, Inc.: Wallingford, CT, 2010.
(45) Dolg, M.; Wedig, U.; Stoll, H.; Preuss, H. *J. Chem. Phys.* **1987**, *86*, 866−872.
(46) Hariharan, P. C.; Pople, J. A. *Theor. chim. Acta* **1973**, *28*, 213−222.
(47) Hehre, W. J.; Ditchfield, R.; Pople, J. A. *J. Chem. Phys.* **1972**, *56*, 2257−2261.
(48) Francl, M. M.; Pietro, W. J.; Hehre, W. J.; Binkley, J. S.; Gordon, M. S.; DeFrees, D. J.; Pople, J. A. *J. Chem. Phys.* **1982**, *77*, 3654−3665.
(49) Barone, V.; Cossi, M. *J. Phys. Chem. A* **1998**, *102*, 1995−2001.
(50) Cossi, M.; Rega, N.; Scalmani, G.; Barone, V. *J. Comput. Chem.* **2003**, *24*, 669−681.
(51) Bondi, A. *J. Phys. Chem.* **1964**, *68*, 441−451.
(52) Floris, F.; Tomasi, J. *J. Comput. Chem.* **1989**, *10*, 616−627.
(53) Floris, F. M.; Tomasi, J.; Pascual Ahuir, J. L. *J. Comput. Chem.* **1991**, *12*, 784−791.
(54) Pierotti, R. A. *Chem. Rev.* **1976**, *76*, 717−726.
(55) Ribeiro, R. F.; Marenich, A. V.; Cramer, C. J.; Truhlar, D. G. *J. Phys. Chem. B* **2011**, *115*, 14556−14562.
(56) Auer, B.; Fernandez, L. E.; Hammes-Schiffer, S. *J. Am. Chem. Soc.* **2011**, *133*, 8282−8292.
(57) Galan, B. R.; Schöffel, J.; Linehan, J. C.; Seu, C.; Appel, A. M.; Roberts, J. A. S.; Helm, M. L.; Kilgore, U. J.; Yang, J. Y.; DuBois, D. L.; Kubiak, C. P. *J. Am. Chem. Soc.* **2011**, *133*, 12767−12779.
(58) Yang, J. Y.; Bullock, R. M.; Shaw, W. J.; Twamley, B.; Fraze, K.; Rakowski DuBois, M.; DuBois, D. L. *J. Am. Chem. Soc.* **2009**, *131*, 5935−5945.
(59) Solis, B. H.; Hammes-Schiffer, S. *Inorg. Chem.* **2011**, *50*, 11252−11262.
(60) Kilgore, U. J.; Roberts, J. A. S.; Pool, D. H.; Appel, A. M.; Stewart, M. P.; Rakowski DuBois, M.; Dougherty, W. G.; Kassel, W. S.; Bullock, R. M.; DuBois, D. L. *J. Am. Chem. Soc.* **2011**, *133*, 5861−5872.
(61) Kilgore, U. J.; Stewart, M. P.; Helm, M. L.; Dougherty, W. G.; Kassel, W. S.; Rakowski DuBois, M.; DuBois, D. L.; Bullock, R. M. *Inorg. Chem.* **2011**, *50*, 10908−10918.
(62) Pourbaix, M. *Atlas of Electrochemical Equilibria in Aqueous Solutions*, 2nd ed.; NACE International: Houston, TX, 1974.